


RESEARCH ARTICLE

Alleviating Substrate Inhibition of Leucine Dehydrogenase by Enhancing NAD⁺ Dissociation Efficiency

Jun-Ping Zhou^{1,2} | Yi-Nan Xue² | Feng Wang² | Hui Gao² | Zhi-Cheng Zhang² | Ai-Ping Pang^{1,2} | Zhi-Qiang Liu^{1,2}  | Yu-Guo Zheng^{1,2}

¹The National and Local Joint Engineering Research Center for Biomanufacturing of Chiral Chemicals, Zhejiang University of Technology, Hangzhou, China | ²Key Laboratory of Bioorganic Synthesis of Zhejiang Province, College of Biotechnology and Bioengineering, Zhejiang University of Technology, Hangzhou, China

Correspondence: Zhi-Qiang Liu (microlu@zjut.edu.cn)

Received: 13 February 2025 | **Revised:** 24 April 2025 | **Accepted:** 8 May 2025

Funding: This study was supported by the National Key Research and Development Program of China (2022YFA0911800), National Key Research and Development Program of China, National Natural Science Foundation of China (32101170), and Zhejiang Province Postdoctoral Research Project Preferential Funding (ZJ2023159).

Keywords: 2-oxobutyric acid | L-2-aminobutyric acid | leucine dehydrogenase | NAD⁺ dissociation | substrate inhibition

ABSTRACT

Leucine dehydrogenase catalyzes the asymmetric reductive amination of ketoacids to produce valuable chiral unnatural amino acids, but its application is often constrained by substrate inhibition. Here we employed a rational engineering strategy to alleviate substrate inhibition by enhancing the dissociation efficiency of NAD⁺. Notably, the variant H184A exhibited a 1.53-fold increase in enzyme activity and a 58% improvement in the half-maximal inhibitory concentration for 2-oxobutyric acid, alleviating substrate inhibition.

1 | Introduction

Unnatural amino acids (UAAs) usually serve as key chiral precursors for the synthesis of several important drugs, such as L-2-aminobutyric acid (L-2-ABA), which can be used for antiepileptic drug levetiracetam production [1]. UAAs can be synthesized from ketoacids by asymmetric reductive amination [2], a reaction that, when catalyzed by enzymes, offers advantages over chemical catalysis, including higher stereoselectivity, superior chemo- and regioselectivity, higher turnover rates, and milder reaction conditions [3]. Here, the key enzyme leucine dehydrogenase (LeuDH), which has been widely applied in the synthesis of UAAs due to its broad substrate specificity [4–6], was studied using L-2-ABA as an example (Figure 1). Due to the high cost of substrate 2-OBA, the conventional method for L-2-ABA biosynthesis involves a two-step enzymatic process including deamination by threonine deaminase (TD), and reductive amination by LeuDH, with bulk

L-threonine (L-Thr) as the substrate [7–9]. This pathway has been successfully implemented in *Saccharomyces cerevisiae* [10] and *Escherichia coli* [11] for L-2-ABA production. However, despite various types of LeuDHs being screened to enhance L-2-ABA synthesis, a significant challenge remains: LeuDH is severely inhibited by the substrate 2-oxobutyric acid (2-OBA) [12, 13]. This substrate inhibition commonly occurs in natural hydroxyacid dehydrogenases, as high concentrations of ketoacid substrates can form a non-productive enzyme-NAD⁺-ketoacid ternary complex, reducing the enzyme activity [14]. Therefore, exploring strategies to alleviate substrate inhibition of LeuDH could not only improve the industrial production of L-2-ABA, but also offer valuable insights for relieving substrate inhibition for other similar NAD(P)H-dependent dehydrogenases.

The monomer of amine dehydrogenases (AmDHs) typically consists of two domains: a Rossmann fold domain at the N-

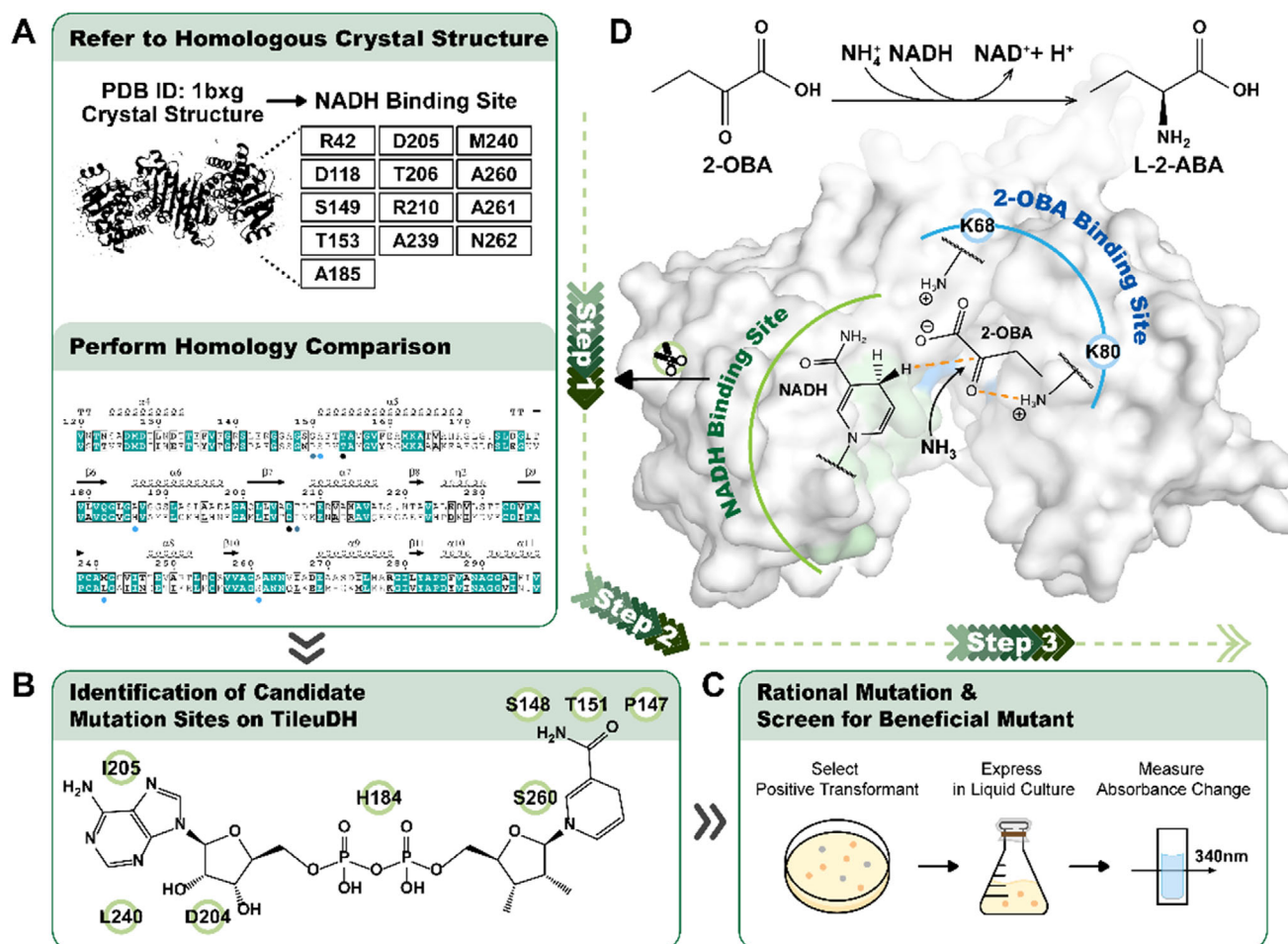


FIGURE 1 | The flowchart for rational engineering. (A) The NAD⁺/NADH binding site was identified as the engineering target by alignment of the *Ti*LeuDH modeling structure with the known crystal structure of the holo-form of PheDH (PDB ID: 1bxxg). (B) Eight potential residues were selected for rational mutagenesis and (C) beneficial variants were then screened by monitoring absorbance changes at 340 nm. (D) The reductive amination reaction of LeuDH for converting 2-OBA to L-2-ABA, and the structure of *Ti*LeuDH modeled by AlphaFold3, as further detailed in Section 3.1.

terminal for coenzyme binding, and a six-strand β -sheet domain at the C-terminal for substrate binding [3], separated by a deep cleft containing the active site [5]. LeuDH follows this general structure, with the substrate 2-OBA binding to Lys68 and Lys80 in the C-terminal domain [15, 16], and NAD⁺/NADH binding to the N-terminal domain. To improve the industrial characteristics of LeuDH, several studies have focused on its thermal stabilities, substrate specificities, and other properties. These efforts include modifying the substrate-binding region to alter substrate specificities [5, 17–20], engineering flexible regions to enhance thermal stability [21], increasing coenzyme affinity to improve catalytic efficiencies [6], and even designing chimeric enzyme by combining the strong NAD⁺/NADH-affinity domain from LeuDH with the substrate-binding domain of phenylalanine dehydrogenase (PheDH) for better catalytic performance [22]. However, substrate inhibition, especially by 2-OBA, has rarely been addressed in LeuDH [12, 13]. Although some studies used directed evolution to screen LeuDH variants that reduce 2-OBA inhibition, the residues for mutagenesis were primarily located in the substrate-binding domain [23]. None of the literature considered the substrate alleviation by enhancing NAD⁺ dissociation efficiency, which may not only increase the

enzymatic turnover rate but also accelerate cofactor regeneration, which is a key factor for the efficient biosynthesis of valuable chemicals [24, 25].

Here, we highlight the potential of modifying the coenzyme-binding domain of LeuDH to enhance NAD⁺ dissociation efficiency, thereby alleviating substrate inhibition. The LeuDH we engineered was from *Thermoactinomyces intermedius* (*Ti*LeuDH) [26], which exhibited higher enzyme activity for L-2-ABA synthesis in our previous study [11]. Here, modeling structure of *Ti*LeuDH was aligned with the crystal structure of the holo-form of PheDH binding NADH (PDB: 1bxxg), and eight candidate sites in the NAD⁺/NADH-binding domain of *Ti*LeuDH were selected for rational mutation (P147S, S148L, T151L, H184A, D204A, I205T, L240M, and S260A) (Figure 1A–C). By monitoring the absorbance change at 340 nm, H184A and S260A showed higher activity than the WT. Both variants were rationally designed to weaken the binding of NAD⁺/NADH, thereby enhancing NAD⁺ dissociation efficiency. The two beneficial variants were then identified and analyzed *in vitro*, *in vivo*, and *in silico* to further understand their characteristics. The mechanisms underlying these changes provide a novel strategy to overcome ketoacid-induced

substrate inhibition in dehydrogenases by improving coenzyme dissociation efficiency, which reduces substrate inhibition by accelerating enzyme-NAD⁺-ketoacid ternary complex dissociation.

2 | Materials and Methods

2.1 | Strains, Vectors, and Chemicals

The *Tldh* gene encoding *Ti*LeuDH (Uniprot Accession: Q60030) from *T. intermedius* was studied [26]. *E. coli* BL21 (DE3) was used for protein expression. *E. coli* THR was previously constructed as an L-Thr-producing strain in our lab [11], and used as the host cell for L-2-ABA fermentation. The plasmid pET-28a (Novagen Co., Darmstadt, Germany) was employed as an expression vector. The plasmid pTrc99A-Pbs-*ilvA**-Gap-*Tldh* was used in *E. coli* THR to test the *Ti*LeuDH variants. Primers were synthesized by Qingke Biotechnology Ltd. (Hangzhou, China). The substrate 2-OBA sodium salt and coenzyme NADH were purchased from Aladdin. L-Thr and L-2-ABA were purchased from Macklin. Isopropyl- β -D-thiogalactoside (IPTG) was purchased from Beyotime Biotechnology (Shanghai, China). All other chemicals of high grade were obtained from commercial sources.

2.2 | Structural Modeling and Analysis

*Ti*LeuDH bound to NADH was modeled using AlphaFold3 (<https://golgi.sandbox.google.com/>) [27]. The crystal structure of PheDH from *Rhodococcus* sp. (PDB: 1bxg) was downloaded from the PDB database (<http://www.rcsb.org/>) for guidance [28]. Structural analysis of the enzymes was performed using the PyMOL Molecular Graphics System, Version 3.0 Schrödinger, LLC. The substrate 2-OBA was docked with *Ti*LeuDH using DockingPie [29]. $\Delta\Delta G$ -fold values were calculated using FoldX to assess the impact of beneficial mutations on *Ti*LeuDH's folding free energy [30].

2.3 | Variant Constructions, Enzyme Expressions, and Purifications

*Ti*LeuDH variants were generated using pET28a-*Tldh* as the template, with the wild type referred to as WT. Site-directed mutagenesis was conducted through a one-step PCR method, using the specific primers listed in Table S1. Following PCR, DpnI was employed to digest the template DNA. Positive transformants were selected from LB plates containing 50 μ g/mL kanamycin, and their DNA sequences were further verified by sequencing to exclude false positives. The recombinant strain was initially grown in 10 mL of LB liquid medium as a seed culture, and then transferred to 100 mL of fresh LB liquid medium, where it was incubated at 37°C with shaking at 200 rpm to promote cell growth. When the OD₆₀₀ of the culture reached 0.8, IPTG was added to a final concentration of 1 mM to induce protein expression. The cultures were then incubated at 26°C for 8 h, followed by harvesting through centrifugation at 8000 rpm for 10 min. The harvested cells were resuspended in 50 mM PBS buffer (pH 7.5) and treated with ultrasonication for cell disruption. The

resulting crude enzyme extract was obtained by centrifugation at 10,000 rpm for 20 min at 4°C. Protein purification was performed using a nickel-NTA affinity column (Ni²⁺ column). The purity of the enzymes was assessed via Coomassie brilliant blue staining of SDS-PAGE gels (Figure S1). Protein concentrations were measured at room temperature using the Bradford method with BSA as the standard.

2.4 | Enzyme Activity, 2-OBA Tolerance, and Biochemical Characterization

Enzyme activities were measured by monitoring the consumption of NADH during the reductive amination reaction. The absorbance changes at 340 nm were recorded every 15 s for 2 min using a spectrophotometer [31]. The reaction mixture (2 mL) contained NH₄OH-NH₄Cl buffer (900 mM, pH 9.5), 2-OBA (1.2 g/L), NADH (0.1 mM), and an appropriate amount of crude enzyme. One unit of *Ti*LeuDH activity was defined as the amount of enzyme required to catalyze the consumption of 1 mmol of NADH per minute under assay conditions.

The procedure for determining 2-OBA tolerance was similar to the enzyme activity assay, but with the pH of the NH₄OH-NH₄Cl buffer adjusted to 7.5 to monitor the intracellular pH and the 2-OBA concentration varied from 0.1 to 15 g/L, using purified enzymes. The optimal temperature for *Ti*LeuDH activity was determined by testing temperatures ranging from 30°C to 70°C. The optimal pH for *Ti*LeuDH was assessed over a pH range from 5.5 to 10. Thermostability was evaluated by incubating the purified enzyme at 60°C for 72 h, followed by measuring the residual enzyme activities. The protein's melting temperature (*T*_m) was determined by recording its thermal denaturation process using a circular dichroism (CD) spectrometer with a temperature control system. All the fitting curves were fitted using Origin.

2.5 | Fermentation of Recombinant *E. coli* THR/pTrc99A-Pbs-*ilvA**-Gap-*Tldh* for L-2-ABA Production in Shake Flask

The template plasmid pTrc99A-Pbs-*ilvA**-Gap-*Tldh* for variants to generate was constructed in our previous studies [11]. The L-Thr-producing-strain *E. coli* THR used to express the plasmid was also constructed in our previous studies [11]. The beneficial *Ti*LeuDH variants H184A and S260A were introduced into the plasmid pTrc99A-Pbs-*ilvA**-Gap-*Tldh*, and the mutated plasmid was then transformed to *E. coli* THR to evaluate the L-2-ABA productions.

The composition of the fermentation medium in a 250 mL flask (30 mL) is as follows: 20 g/L glucose, 14 g/L ammonium sulfate, 6 g/L yeast powder, 4 g/L KH₂PO₄, 4 g/L MgSO₄, 0.025 g/L FeSO₄·7H₂O, 0.020 g/L MnSO₄·1H₂O, 0.022 g/L ZnSO₄·7H₂O, and CaCO₃ 0.5 g/L. Before inoculation, 30 mL of fermentation medium was supplemented with filter-sterilized ampicillin and IPTG, both at a final concentration of 0.1 mM. The inoculation rate was 1%, and the fermentation broth was cultivated at 33°C for 48 h.

2.6 | HPLC Analysis

The concentrations of L-Thr and L-2-ABA were determined using an Agilent LC1260 HPLC system with phenylisothiocyanate (PITC) derivatization method. Samples were manually derivatized using PITC before injection onto the column, with the following procedure: the sample (200 μ L) was mixed with 1 M triethylamine-acetonitrile solution (100 μ L) and 0.2 M PITC-acetonitrile solution (100 μ L), then incubated at room temperature for 1 h. 400 μ L of n-hexane was then added to remove the remaining PITC. The aqueous phase (200 μ L) was collected and mixed with 800 μ L of water for analysis. The mobile phases required for HPLC detection consisted of Phase A and Phase B. Phase A was a 0.05 M sodium acetate aqueous solution, with the pH adjusted to 6.50 ± 0.05 using acetate. Phase B contained methanol, acetonitrile, and water in a volume ratio of 1:3:1. The chromatographic conditions were as follows: a C18 column (5 μ m, 4.6*250 mm) maintained at 45°C, with a flow rate of 1 mL/min and sample measured at 254 nm. A gradient elution was performed with Phases A and B. The initial conditions for gradient elution were 95% phase A and 5% phase B. Over the first 20 min, Phase A was gradually decreased to 52%. From 21 to 25 min, Phase B was maintained at 100%. Finally, the column was equilibrated with 95% Phase A and 5% Phase B for the next cycle.

2.7 | MD Simulation

MD simulations were performed to evaluate the dynamic behavior and stability of the *Ti*LeuDH WT and its variants, H184A and S260A. The structural models of the *Ti*LeuDH variants were prepared and imported into GROMACS for simulation. Each protein-coenzyme complex was solvated in a cubic water box using the TIP3P water model, with a minimum distance of 1.0 nm between the protein and the box boundary. Sodium (Na^+) and chloride (Cl^-) ions were added to neutralize the system, followed by energy minimization to resolve steric clashes and optimize the initial configuration.

The simulations included a 50 ns production run at 300 K with a time step of 2 fs, after initial thermal and pressure equilibration. Simulation trajectories were analyzed to calculate the root-mean-square deviation (RMSD) and root-mean-square fluctuation (RMSF) for stability and flexibility assessments, as well as protein-ligand contacts to quantify interactions between the protein and NADH. These analyses provided detailed insights into the structural dynamics and dissociation efficiency between the coenzyme and enzymes.

3 | Results and Discussion

3.1 | Site Mutagenesis Design Toward the NAD^+/NADH Binding Sites of *Ti*LeuDH

AlphaFold3 was used to predict the 3D structure of *Ti*LeuDH and dock it with NADH (Figure S2). The highest-scoring conformation was selected for further analysis, with the guidance from the crystal structure of phenylalanine dehydrogenase (PheDH) from *Rhodococcus* sp. (PDB: 1bxx) [32], as the holo-form of 1bxx with NADH provides detailed insights into the coenzyme-

enzyme interaction sites, which are essential for understanding *Ti*LeuDH's NAD^+/NADH binding mechanisms.

Based on the NAD^+/NADH binding sites in 1bxx and the homology alignment between *Ti*LeuDH and 1bxx, we selected the following candidate residues in *Ti*LeuDH for rational modification: P147, S148, T151, H184, D204, I205, L240, and S260 (Figure 2A,B). Our goal is to enhance NAD^+ dissociation by rationally modifying these residues, which could influence the dissociation efficiency of the enzyme- NAD^+ -ketoacid ternary complex, thereby altering the level of substrate inhibition [14].

To promote NAD^+ dissociation, we mutated residues that potentially form hydrogen bonds with NAD^+/NADH to amino acids incapable of forming hydrogen bonds: S148L, T151L, H184A, D204A, L240M, and S260A. Among these candidate residues, two conserved residues—T151 (T153 in 1bxx) and D204 (D205 in 1bxx)—are predicted to interact with NAD^+/NADH in a manner similar to the interactions observed in 1bxx. Specifically, the O' of T151 forms a hydrogen bond with the carboxamide oxygen of the nicotinamide, while the carboxylate group of D204 interacts with the 2'-hydroxyl group of the adenine ribose [32]. Since these interactions are critical for NAD^+/NADH coupling in *Ti*LeuDH, weakening them may lead to enzyme inactivation, which requires further validation.

To further explore the relationship between NAD^+/NADH binding strength and substrate inhibition, P147 (weakly conserved with S149 in 1bxx) and I205 (weakly conserved with T206 in 1bxx) in *Ti*LeuDH were mutated to P147S and I205T, respectively, based on the 1bxx structure, where S149 and T206 are known to form hydrogen bonds with NAD^+/NADH . Based on our hypothesis that enhancing NAD^+ dissociation improves the dissociation efficiency of the enzyme- NAD^+ -ketoacid ternary complex, we propose that introducing additional hydrogen bonds may negatively impact enzyme activity by hindering NAD^+ release.

3.2 | Screening and Characterization of Beneficial Variants

Crude enzyme extracts of *Ti*LeuDH WT and its variants were measured for their enzyme activities, and those enzymes displaying residual activity were subsequently purified for further characterization. Enzyme activity was measured using a spectrophotometer to monitor NADH consumption during reductive amination at 340 nm [31]. After screening, three variants retained activity after mutation, while the activities of the other variants were undetectable (Figure 2C). The variants P147S, S148L, T151L, D204A, and L240M, with undetectable enzymatic activities, were first designed to alter interactions with the nicotinamide (head) and adenine (tail) groups of NADH. Results suggested that interactions at both side groups of the NADH molecule played a critical role in stabilizing the enzyme and maintaining its catalytic activity, as either weakened or overly strong interactions would lead to enzyme inactivation. Among the active variants, H184A and S260A, designed to enhance NAD^+ dissociation, demonstrated enhanced activities of 1.53-fold and 1.10-fold compared to that of the WT, respectively. In contrast, the I205T variant, designed to reduce NAD^+ dissociation, showed declined activity.

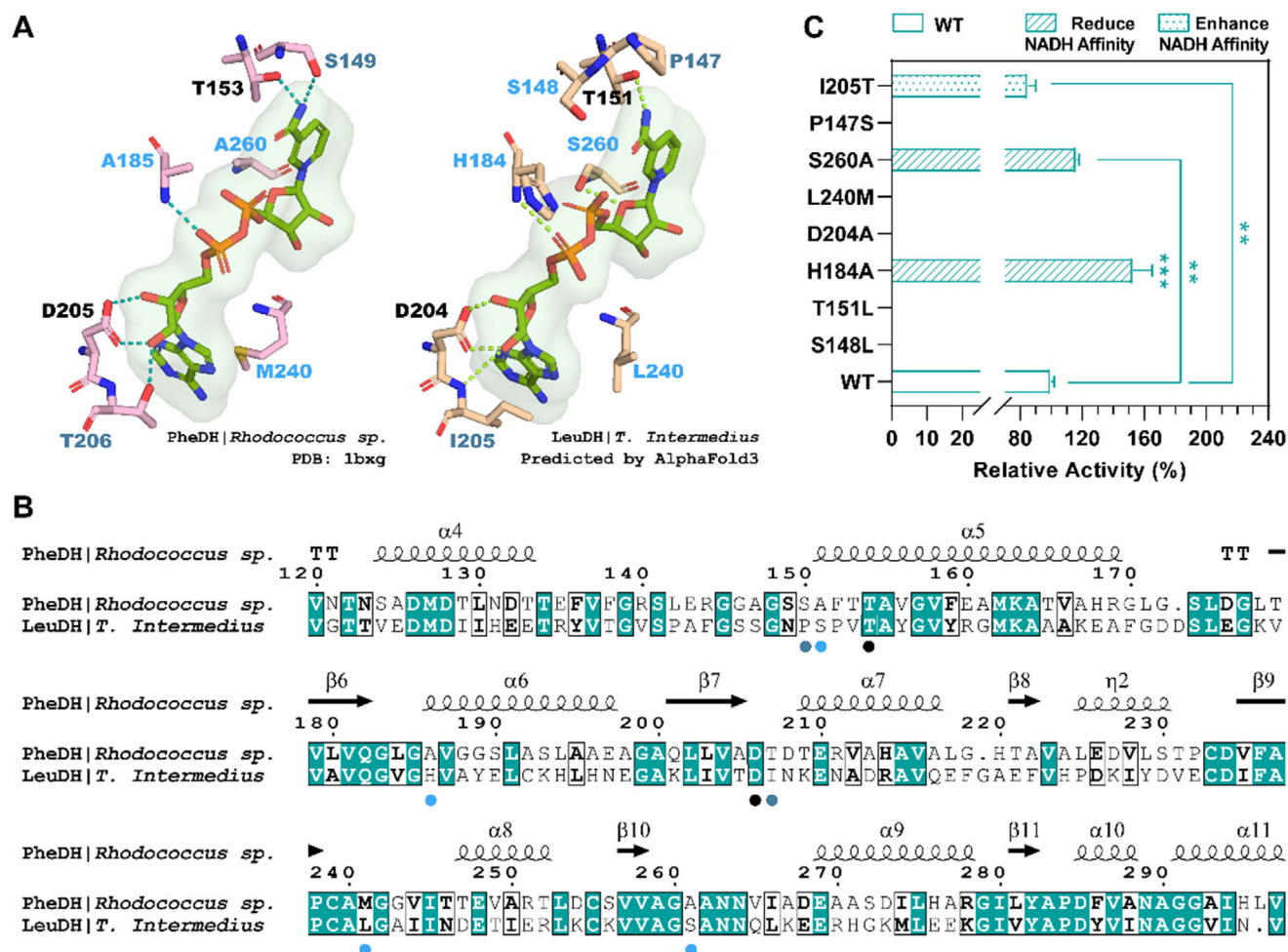


FIGURE 2 | Residue analysis and screening results for rational engineering of *TiLeuDH*. Through comparison with the known crystal structure of the holo-form of PheDH (PDB ID: 1bxg), (A) 3D structural analysis and (B) sequence alignment identified eight residues for rational mutation. Residues marked in light blue were mutated to smaller hydrophobic residues to promote NAD^+ dissociation, dark blue residues were mutated to hydroxylic amino acids to reduce NAD^+ dissociation, and black residues, as conserved sites, were mutated to smaller hydrophobic amino acids to verify their key roles in the NAD^+/NADH binding site. Hydrogen bonds shown in blue were based on the crystal structure, while those in green were predicted from the modeled structure. Subsequently, (C) the variants P147S, S148L, T151L, H184A, D204A, I205T, L240M, and S260A were screened by monitoring absorbance changes at 340 nm, with the WT set at 100% activity for comparison of relative enzymatic activity among variants.

TABLE 1 | Relative enzyme activity (EA), half-maximal inhibitory concentration, and T_m values of *TiLeuDH* and its beneficial variants.

Type	Relative EA ^a (%)	6 h residual EA ^a (%)	IC_{50} (g/L)	T_m (°C)	ΔT_m (°C)
WT	100.0	57.6	~8.0	63.3 ± 0.1	0.0
H184A	153.0	80.6	~12.6	62.6 ± 0.1	-0.7
S260A	109.8	76.0	~9.0	64.2 ± 0.1	+0.9
I205T	84.9	70.9	~7.7	64.9 ± 0.1	+1.6

^aRelative EA was calculated by setting the NADH consumption of the WT as 100%. The 6 h residual EA was calculated by setting each enzyme's 0 h residual EA as 100%.

The correlation between enzyme activity and NAD^+/NADH -affinity, as shown above, prompted us to investigate variations in 2-OBA tolerance among these variants. Thus, the 2-OBA tolerance curves for the four enzymes (WT, H184A, S260A, and I205T) were determined, and the half-maximal inhibitory concentration (IC_{50}) was used to assess the 2-OBA tolerance of

each enzyme. As shown in Table 1 and Figure 3A, the IC_{50} values of the two NAD^+/NADH -affinity-reducing variants increased, while the IC_{50} values of the NAD^+/NADH -affinity-enhancing variant decreased, directly supporting the idea that accelerating NAD^+ dissociation could help alleviate substrate inhibition. Among them, the H184A variant exhibited a 158% increase in IC_{50}

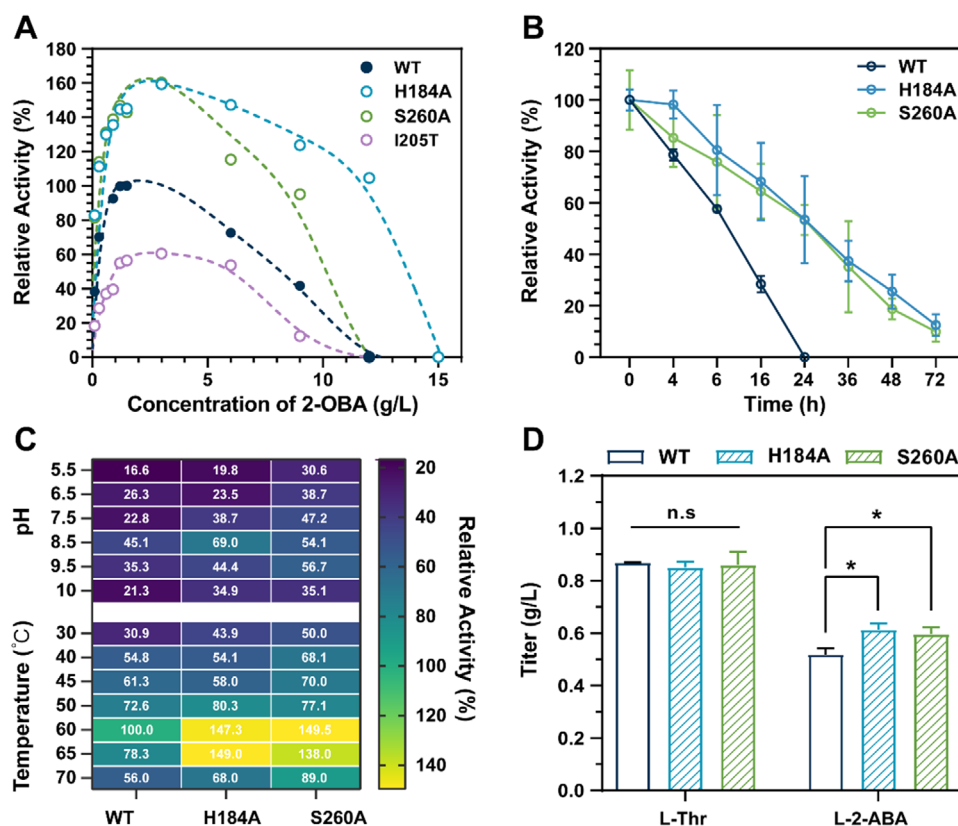


FIGURE 3 | Enzymatic properties of *TiLeuDh* and its variants. (A) Tolerance to different 2-OBA concentrations. (B) Thermal stabilities of the WT *TiLeuDh* and its variants under 60°C incubations for different time. (C) Optimal pH and temperature ranges. (D) Results of 250 mL flask fermentation for L-2-ABA productions.

compared to the WT, reaching approximately 12.6 g/L, indicating its potential for further application in L-2-ABA biosynthesis. However, when the 2-OBA concentration exceeded 12 g/L, even the high-activity variants displayed a sharp decrease in enzyme activity. This suggests that substrate inhibition is a complex phenomenon, potentially related to the dissociation efficiency of the entire enzyme-NAD⁺-ketoacid ternary complex. Therefore, unlike the reference [14], the efficiency of substrate dissociation might also need to be considered when aiming to fully overcome substrate inhibition in *TiLeuDh*.

Subsequently, further characterization was performed on the WT and the two well-performing variants, H184A and S260A. The three enzymes were incubated at 60°C to test their thermal stabilities (Figure 3B). The WT maintained 57.6% activity after 6 h of incubation, while H184A and S260A retained 80.6% and 76.0% activity, respectively, indicating their better thermostabilities, which was further supported by the calculated $\Delta\Delta G$ -fold values (H184A: -0.6 kcal/mol, S260A: -1.1 kcal/mol). The enhanced stabilities of these two beneficial variants may be related to the increased structural rigidities resulting from improved hydrophobicities after the mutation of histidine and serine (which can form hydrogen bonds with NAD⁺/NADH) to alanine.

To further comprehensively understand the enzymatic characteristics of the two beneficial variants, we assessed their optimal temperature, optimal pH, and T_m , comparing them with the WT (Figure 3C). The trends for optimal temperature and pH were similar across all three enzymes, with optimal pH ranging from

8.5 to 9.5 and optimal temperature ranging from 60°C to 65°C. But, when compared at the same pH or temperature, enzyme activity followed the order: H184A > S260A > WT.

The T_m values of WT, H184A, S260A, and the catalytically impaired variant I205T were assessed by circular dichroism (CD) spectroscopy. Compared to WT, H184A showed a slightly lower T_m , while both S260A and I205T exhibited higher T_m values. However, their structural changes differed (Figure S3): S260A displayed increased α -helical content, indicating tighter folding, whereas I205T showed a substantial loss of α -helical features despite its enhanced thermostability. These findings suggested that changes of the ligand binding hydrogen bonds could result to the changes of both enzymatic thermal stability and activities.

Finally, we tested the performance of *TiLeuDh* variants H184A and S260A in fermentation using the L-2-ABA production plasmid pTrc99a-Pbs-*ilvA**-Gap-*Tildh* (Figure 3D). The weaker promoter Pbs drives the expression of an endogenous TD variant (TD*, encoded by *ilvA**), and the stronger promoter Gap drives *TiLeuDh*, balancing the two-step conversion of L-Thr to L-2-ABA with 2-OBA as an intermediate. After 48 h of fermentation, all groups accumulated similar L-threonine titers without detectable 2-OBA accumulation. In contrast, the variants H184A and S260A showed significantly higher levels of L-2-ABA productions ($p < 0.05$) compared to the WT, with both achieving approximately 1.2-fold increases and a maximum titer of 0.63 g/L, demonstrating their improved efficiencies and industrial potential (Figure 3D).

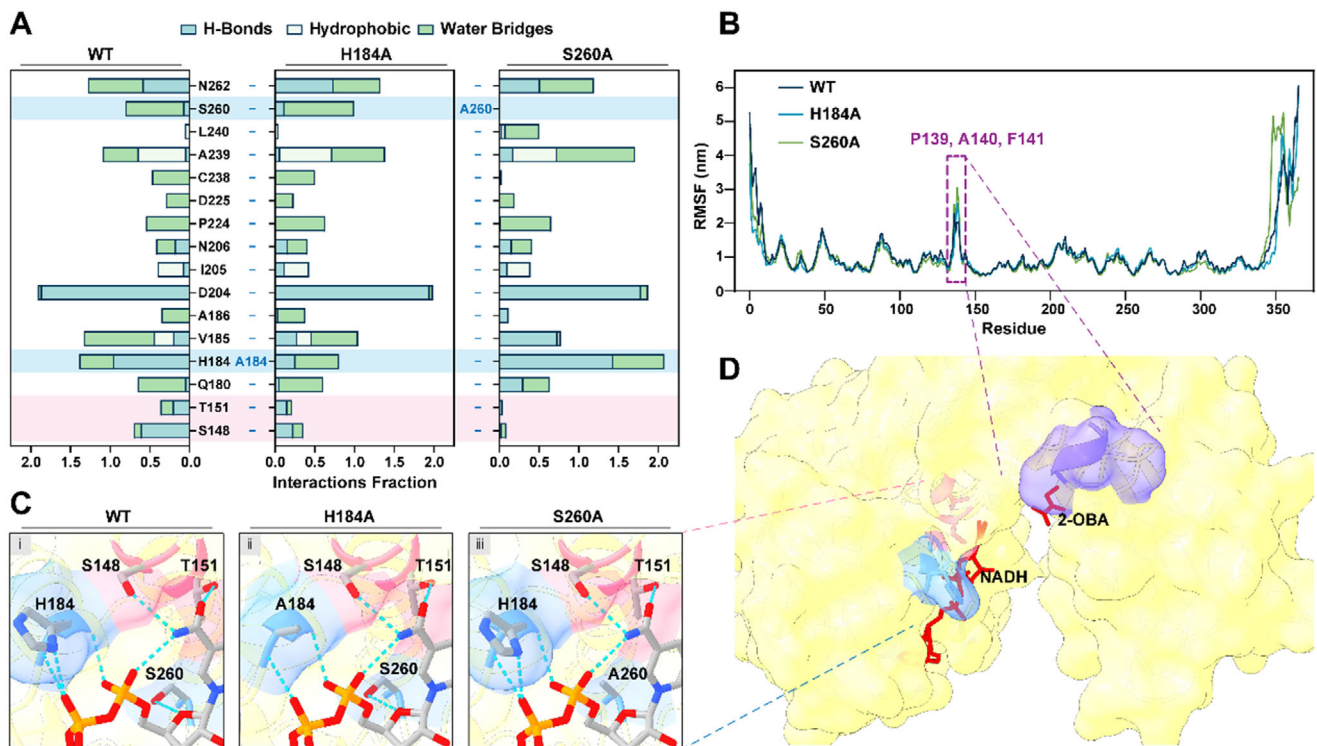


FIGURE 4 | MD simulation and structural analysis of *TiLeuDH* beneficial variants compared to that of the WT. (A) Protein-ligand interactions from MD simulation; (B) RMSF values calculated by MD simulation; (C) Structural comparison of the NADH binding site; (D) Overview of *TiLeuDH*: blue spheres indicate mutated residues (H184, S260), pink spheres mark amino acids near the NADH active site (S148, T151), and purple spheres represent the flexible loop (P139, A140, F141).

3.3 | Structural Analysis of *TiLeuDH* and Its Beneficial Variants

To investigate the mechanism for enhanced NAD⁺ dissociation efficiency that could alleviate 2-OBA inhibition, we conducted 50 ns MD simulations at 300 K for *TiLeuDH* WT and its variants, H184A and S260A (Figure S4). Changes were observed in the interactions between NADH and the mutated *TiLeuDH* (Figure 4A,C). Mutating H184 and S260 to small hydrophobic L-alanine not only reduced their interactions with the middle portion of NADH but also weakened the interactions between NADH's nicotinamide ring and residues T151 and S148 (Figures 4A,C and S5). Although S260A induced a stronger indirect weakening of the binding force between NADH's reactive center and the enzyme, H184A exhibited higher enzymatic activity and a greater ability to alleviate 2-OBA inhibition (Figure 4A,C). This suggested that moderate weakening of the binding force (effective but not excessive) better promoted complex dissociation while maintaining a balanced reaction process.

Additionally, beyond the NAD⁺/NADH binding region, analysis of the calculated root-mean-square fluctuation (RMSF) revealed that both variants showed enhanced flexibilities of the loop (P139, A140, F141) near the substrate channel (Figure 4B,D). Notably, many enzymes achieve activity improvements through modifications of the loop [33], which might influence the release entry of the complex [34]. In summary, increased hydrophobic interactions in the NAD⁺/NADH binding region not only optimized NAD⁺ dissociation but also indirectly improved substrate

entry and exit rate, thereby accelerating the dissociation of the enzyme-NAD⁺-ketoacid complex.

4 | Conclusion

Enhancing the affinity for coenzyme or substrate has been a common strategy for improving the performance of NAD(P)H-dependent enzymes [35]. In this study, we propose a novel approach, emphasizing the often-overlooked dissociation process within the catalytic cycle, as the non-productive abortive ternary complex has been observed in several types of NAD(P)H-dependent dehydrogenases with different substrates, such as lactate dehydrogenase [14] and horse liver alcohol dehydrogenase [36]. While previous efforts have largely focused on improving complex generation, the dissociation efficiency of enzyme-coenzyme-substrate ternary complex is equally critical. Thus, guided by the principle of promoting dissociation, this study demonstrated that weakening the binding force between NAD⁺/NADH and its binding site on *TiLeuDH* could enhance the enzyme activity and alleviate substrate inhibition, with the H184A variant achieving a ~1.5-fold improvement in both activity and substrate tolerance.

Nevertheless, substrate inhibition was not completely resolved, suggesting that further engineering—such as modifying residues in the substrate pocket—might be required. A combined strategy of weakening both NAD⁺/NADH and substrate binding is expected to synergistically accelerate the dissociation of the enzyme-coenzyme-substrate ternary complex, thereby enhanc-

ing the turnover rate and consequently promoting faster cofactor regeneration, which is a key factor for the efficient cofactor-dependent biosynthesis [37]. Furthermore, recent studies have explored identifying robust LeuDH variants from novel sources for efficient L-2-ABA biosynthesis [38], which can serve as promising templates for further enzyme engineering. Overall, our findings highlighted the importance of the often-overlooked dissociation process in enzyme catalysis, offering a new strategy to overcome substrate inhibition and enhance enzyme efficiency. This study provided insights into NAD(P)H-dependent enzyme mechanisms and a foundation for future rational design to improve industrial applications of the NAD(P)H-dependent enzymes.

Author Contributions

Jun-Ping Zhou: experimental design, data analysis, supervision, and the manuscript writing. **Yi-Nan Xue:** experiments, data analysis, computational analysis, and manuscript writing. **Feng Wang:** experiments and data analysis. **Hui Gao:** experiments and data analysis. **Zhi-Cheng Zhang:** experiments. **Ai-Ping Pang:** manuscript review. **Zhi-Qiang Liu:** funding acquisition, supervision. **Yu-Guo Zheng:** funding acquisition.

Acknowledgments

This work was supported by the National Key Research and Development Program of China (2022YFA0911800), National Natural Science Foundation of China (No. 32101170), the Key Research Development Program of Zhejiang Province (2024C03012), and 2023 Zhejiang Province postdoctoral research project preferential funding (ZJ2023159).

Conflicts of Interest

The authors declare no conflicts of interest.

Data Availability Statement

The data that support the findings of this study are available from the corresponding author upon reasonable request.

References

1. K. Zhang, H. Li, K. M. Cho, and J. C. Liao, "Expanding Metabolism for Total Biosynthesis of the Nonnatural Amino Acid L-Homocysteine," *Proceedings of the National Academy of Sciences of the United States of America* 107 (2010): 6234–6239.
2. I. Fotheringham, "Engineering Biosynthetic Pathways: New Routes to Chiral Amino Acids," *Current Opinion in Chemical Biology* 4 (2000): 120–124.
3. B. Yuan, D. Yang, G. Qu, N. J. Turner, and Z. Sun, "Biocatalytic Reductive Aminations With NAD(P)H-Dependent Enzymes: Enzyme Discovery, Engineering and Synthetic Applications," *Chemical Society Reviews* 53 (2024): 227–262.
4. X. Meng, Y. Liu, L. Yang, et al., "Rational Identification of a High Catalytic Efficiency Leucine Dehydrogenase and Process Development for Efficient Synthesis of L-Phenylglycine," *Biotechnology Journal* 18 (2023): 2200465.
5. F. Zhou, Y. Xu, Y. Nie, and X. Mu, "Substrate-Specific Engineering of Amino Acid Dehydrogenase Superfamily for Synthesis of a Variety of Chiral Amines and Amino Acids," *Catalysts* 12 (2022): 380.
6. F. Zhou, X. Mu, Y. Nie, and Y. Xu, "Enhanced Catalytic Efficiency and Coenzyme Affinity of Leucine Dehydrogenase by Comprehensive Screening Strategy for L-Tert-leucine Synthesis," *Applied Microbiology and Biotechnology* 105 (2021): 3625–3634.

7. R. Tao, Y. Jiang, F. Zhu, and S. Yang, "A One-Pot System for Production of L-2-Aminobutyric Acid From L-Threonine by L-Threonine Deaminase and a NADH-Regeneration System Based on L-Leucine Dehydrogenase and Formate Dehydrogenase," *Biotechnology Letters* 36 (2014): 835–841.
8. I. G. Fotheringham, N. Grinter, D. P. Pantaleone, R. F. Senkpeil, and P. P. Taylor, "Engineering of a Novel Biochemical Pathway for the Biosynthesis of L-2-Aminobutyric acid in *Escherichia coli* K12," *Bioorganic & Medicinal Chemistry* 7 (1999): 2209–2213.
9. X. Li, C. Gao, W. Wei, et al., "A Tri-Enzyme Cascade for Efficient Production of L-2-Aminobutyrate From L-Threonine," *ChemBiochem* 24 (2023): 202300148.
10. N. Weber, A. Hatsch, L. Labagnere, and H. Heider, "Production of (S)-2-Aminobutyric Acid and (S)-2-Aminobutanol in *Saccharomyces cerevisiae*," *Microbial Cell Factories* 16 (2017): 51.
11. J. Xu, J. Li, B. Zhang, Z. Liu, and Y. Zheng, "Fermentative Production of the Unnatural Amino Acid L-2-Aminobutyric Acid Based on Metabolic Engineering," *Microbial Cell Factories* 18 (2019): 43.
12. P. Yao, Y. Cui, S. Yu, et al., "Efficient Biosynthesis of (R)- or (S)-2-Hydroxybutyrate From L-Threonine Through a Synthetic Biology Approach," *Advanced Synthesis & Catalysis* 358 (2016): 2923–2928.
13. L. Tian, J. Zhou, T. Yang, X. Zhang, M. Xu, and Z. Rao, "Cascade Biocatalysis for Production of Enantiopure (S)-2-Hydroxybutyric Acid Using Recombinant *Escherichia coli* With a Tunable Multi-Enzyme-Coordinate Expression System," *Systems Microbiology and Biomanufacturing* 1 (2021): 234–244.
14. C. M. Eszes, R. B. Sessions, A. R. Clarke, K. M. Moreton, and J. J. Holbrook, "Removal of Substrate Inhibition in a Lactate Dehydrogenase From Human Muscle by a Single Residue Change," *FEBS Letters* 399 (1996): 193–197.
15. T. Sekimoto, T. Fukui, and K. Tanizawa, "Involvement of Conserved Lysine 68 of *Bacillus stearothermophilus* Leucine Dehydrogenase in Substrate Binding," *Journal of Biological Chemistry* 269 (1994): 7262–7266.
16. T. Sekimoto, T. Matsuyama, T. Fukui, and K. Tanizawa, "Evidence for Lysine 80 as General Base Catalyst of Leucine Dehydrogenase," *Journal of Biological Chemistry* 268 (1993): 27039–27045.
17. J. Lu, Z. Wang, Y. Jiang, Z. Sun, and W. Luo, "Modification of the Substrate Specificity of Leucine Dehydrogenase by Site-Directed Mutagenesis Based on Biocomputing Strategies," *Systems Microbiology and Biomanufacturing* 3 (2023): 384–392.
18. T. Wu, Y. Wang, N. Zhang, et al., "Reshaping Substrate-Binding Pocket of Leucine Dehydrogenase for Bidirectionally Accessing Structurally Diverse Substrates," *ACS Catalysis* 13 (2022): 158–168.
19. J. Zhou, Y. Wang, J. Chen, et al., "Rational Engineering of *Bacillus cereus* Leucine Dehydrogenase Towards α -keto Acid Reduction for Improving Unnatural Amino Acid Production," *Biotechnology Journal* 14 (2019): 1800253.
20. X. Yin, W. Gong, Y. Zeng, et al., "Substrate-Specific Evolution of Amine Dehydrogenases for Accessing Structurally Diverse Enantiopure (R)- β -Amino Alcohols," *ACS Catalysis* 14 (2024): 837–845.
21. X. Zhang, X. Zhang, H. Shi, et al., "Combining Flexible Region Design and Automatic Design to Enhance the Thermal Stability and Catalytic Efficiency of Leucine Dehydrogenase," *Journal of Agricultural and Food Chemistry* 72 (2024): 13801–13811.
22. J. Li, X. Mu, T. Wu, and Y. Xu, "High Coenzyme Affinity Chimeric Amine Dehydrogenase Based on Domain Engineering," *Bioresources and Bioprocessing* 9 (2022): 33.
23. J. Chen, R. Zhu, J. Zhou, et al., "Efficient Single Whole-Cell Biotransformation for L-2-Aminobutyric Acid Production Through Engineering of Leucine Dehydrogenase Combined With Expression Regulation," *Bioresource Technology* 326 (2021): 124665.
24. W. Ma, F. Li, L. Li, et al., "Production of D-Tagatose, Bioethanol, and Microbial Protein From the Dairy Industry By-Product Whey Pow-

der Using an Integrated Bioprocess," *Biotechnology Journal* 19 (2024): 2300415.

25. S. Zou, B. Zhang, Y. Han, et al., "Design of a Cofactor Self-Sufficient Whole-Cell Biocatalyst for Enzymatic Asymmetric Reduction via Engineered Metabolic Pathways and Multi-Enzyme Cascade," *Biotechnology Journal* 19 (2024): 2300744.

26. T. Ohshima, N. Nishida, S. Bakthavatsalam, et al., "The Purification, Characterization, Cloning and Sequencing of the Gene for a Halostable and Thermostable Leucine Dehydrogenase From *Thermoactinomyces intermedius*," *European Journal of Biochemistry* 222 (1994): 305–312.

27. J. Abramson, J. Adler, J. Dunger, et al., "Accurate Structure Prediction of Biomolecular Interactions With AlphaFold 3," *Nature* 630 (2024): 493–500.

28. N. M. Brunhuber, J. B. Thoden, J. S. Blanchard, and J. L. Vanhooke, "Rhodococcus L-Phenylalanine Dehydrogenase: Kinetics, Mechanism, and Structural Basis for Catalytic Specificity," *Biochemistry* 39 (2000): 9174–9187.

29. S. Rosignoli and A. Paiardini, "DockingPie: A Consensus Docking Plugin for PyMOL," *Bioinformatics* 38 (2022): 4233–4234.

30. J. Schymkowitz, J. Borg, F. Stricher, R. Nys, F. Rousseau, and L. Serrano, "The FoldX Web Server: An Online Force Field," *Nucleic Acids Research* 33 (2005): W382–388.

31. M. Klingenberg, "Nicotinamide-Adenine Dinucleotides (NAD, NADP, NADH, NADPH): Spectrophotometric and Fluorimetric Methods," in: *Methods of Enzymatic Analysis*, 2nd ed., ed. H. U. Bergmeyer (Academic Press), 4 (1974): 2045–2072.

32. J. L. Vanhooke, J. B. Thoden, N. M. W. Brunhuber, J. S. Blanchard, and H. M. Holden, "Phenylalanine Dehydrogenase From *Rhodococcus* Sp. M4: High-Resolution X-Ray Analyses of Inhibitory Ternary Complexes Reveal Key Features in the Oxidative Deamination Mechanism," *Biochemistry* 38 (1999): 2326–2339.

33. T. Zhou, X. Li, X. Zhang, X. Cai, Z. Liu, and Y. Zheng, "Improving the Catalytic Performance of Carbonyl Reductase Based on the Functional Loops Engineering," *Biotechnology and Bioengineering* 122 (2025): 167–178.

34. Q. Ma, X. Wang, F. Luan, et al., "Functional Studies on an Indel Loop Between the Subtypes of *Meso*-Diaminopimelate Dehydrogenase," *ACS Catalysis* 12 (2022): 7124–7133.

35. X. Meng, L. Yang, Y. Liu, H. Wang, Y. Shen, and D. Wei, "Identification and Rational Engineering of a High Substrate-Tolerant Leucine Dehydrogenase Effective for the Synthesis of L-*tert*-Leucine," *Chemcatchem* 13 (2021): 3340–3349.

36. A. Vetrano, M. Capone, M. Farina, F. Gabriele, N. Spredi, and I. Daidone, "Unveiling Cofactor Inhibition Mechanisms in Horse Liver Alcohol Dehydrogenase: An Allosteric Driven Regulation," *Bioorganic Chemistry* 153 (2024): 107932.

37. N. Wu, X. Wu, M. Zhang, C. Zhang, and Q. Xu, "Metabolic Engineering of *Aspergillus niger* for Accelerated Malic Acid Biosynthesis by Improving NADPH Availability," *Biotechnology Journal* 19 (2024): 2400014.

38. Y. Liu, X. Zhong, Z. Luo, et al., "The Identification of a Robust Leucine Dehydrogenase From a Directed Soil Metagenome for Efficient Synthesis of L-2-Aminobutyric Acid," *Biotechnology Journal* 18 (2023): 2200590.

Supporting Information

Additional supporting information can be found online in the Supporting Information section.